Article

Electrodeposition of Copper Oxides as Cost-Effective Heterojunction Photoelectrode Materials for Solar Water Splitting

Tai-Hsin Yin [1,†], **Bu-Jine Liu [1,†]**, **Yu-Wei Lin [1]**, **Yi-Syuan Li [1]**, **Chih-Wei Lai [1]**, **Yu-Pin Lan [1]**, **Changsik Choi [2,*]**, **Han-Chen Chang [3,*]** and **YongMan Choi [1,*]**

1   College of Photonics, National Yang Ming Chiao Tung University, Tainan 71150, Taiwan
2   Clean Energy Conversion Research Center, Institute for Advanced Engineering, Yongin 17180, Republic of Korea
3   Green Energy and Environment Research Laboratories, Industrial Technology Research Institute, Tainan 71150, Taiwan
*   Correspondence: cschoi@iae.re.kr (C.C.); yessey@itri.org.tw (H.-C.C.); ymchoi@nycu.edu.tw (Y.C.)
†   These authors contributed equally to this work.

Abstract: Photoelectrocatalytic hydrogen production is crucial to reducing greenhouse gas emissions for carbon neutrality and meeting energy demands. Pivotal advances in photoelectrochemical (PEC) water splitting have been achieved by increasing solar light absorption. P-type Cu-based metal oxide materials have a wide range of energy band gaps and outstanding band edges for PEC water splitting. In this study, we first prepared Cu_2O thin films using electrodeposition and fabricated a heterojunction structure of CuO/Cu_2O by controlling annealing temperatures. The surface morphological, optical, and electrochemical properties were characterized using various analytical tools. X-ray and Raman spectroscopic approaches were used to verify the heterojunction of CuO/Cu_2O, while surface analyses revealed surface roughness changes in thin films as the annealing temperatures increased. Electrochemical impedance spectroscopic measurements in conjunction with the Mott–Schottky analysis confirm that the CuO/Cu_2O heterojunction thin film can boost photocurrent generation ($1.03 \ \mathrm{mA/cm^2}$ at 0 V vs. RHE) via enhanced light absorption, a higher carrier density, and a higher flat band potential than CuO and Cu_2O thin films (0.92 and $0.08 \ \mathrm{mA/cm^2}$, respectively).

Keywords: p-type semiconductor; copper oxide; heterojunction; electrodeposition; photoelectrochemical water splitting

1. Introduction

Solar energy is one of the most viable renewable energy resources to meet global energy demand and minimize environmental pollution and global warming [1]. Effective solar energy harvesting has been a central direction in improving photoconversion efficiencies [2–4]. Among solar energy-driven approaches for producing green hydrogen, photoelectrochemical (PEC) water splitting has attracted significant attention [5]. Briefly, it generates electron-hole pairs via a semiconductor photoelectrode by absorbing sunlight and separating the charges that go to the photoelectrodes. Then, the reduction and oxidation processes of water on the electrodes by charge carriers occur, producing hydrogen and oxygen [6]. To date, many photoelectrode materials for PEC water splitting have been designed, including TiO_2 [7,8], Fe_2O_3 [9,10], $BiVO_4$ [11,12], Si [13,14], Cu_2O [15,16], and CuO [17,18]. Photoelectrodes for PEC water splitting must have a suitable energy band gap [5]. For example, the energy of the conduction band (CB) should be lower than that of reduced water, while that of the valence band (VB) should be higher than that of oxidized water. In particular, p-type semiconducting copper oxides (i.e., Cu_2O and CuO) have a low energy band gap (2.0–2.5 eV [19–21] and 1.3–2.1 eV [20,22,23], respectively). It is also

known that they are a potential electrode material for photovoltaic applications [24] because of their cost-effectiveness, non-toxicity, excellent carrier mobility [25], and high absorption coefficient. Similarly, these advantages make copper oxides suitable as an efficient photo-electrode for PEC water splitting, as shown in Table S1 [26–37] and Table S2 [38–40]. One crucial obstacle to copper oxides may be their high electron-hole recombination rate, lowering photoconversion efficiencies. One of the effective approaches to address the issue is to employ a heterostructure configuration with a non-copper-containing semiconductor material, for example, Fe_2O_3/CuO [41,42], CuO/ZnO [43], TiO_2/CuO [44], WO_3/Cu_2O [45], InGaN/Cu_2O [46], and Cu_2O/g-C_3N_4/Cu_2O [47]. Although the heterojunction structures reduce the electron-hole recombination rate, they also increase the complexity of devices. Accordingly, heterostructured CuO/Cu_2O, which has been proposed as the heterojunction configuration, can be prepared using simple thermal oxidation from Cu_2O (Cu_2O + $1/2O_2 \rightarrow 2CuO$) [28]. In this work, we reported a facile method to prepare a CuO/Cu_2O heterojunction structure for PEC water splitting. Cu_2O thin films were prepared by electrodeposition, and thermal treatment was performed [28,40,48]. Simple and eco-friendly electrodeposition by controlling annealing temperatures resulted in micron thick copper oxide layers (~1.4 μm thick) compared to physical methods (i.e., sputtering and pulsed laser deposition). Controlling thin-film thicknesses is one of the essential design factors to improve electron-hole separation [49,50]. The heterojunction configuration demonstrated improved PEC performance compared to CuO and Cu_2O, as confirmed by the analysis of X-ray diffraction (XRD), X-ray photoelectron spectroscopy (XPS), ultraviolet-visible (UV-Vis) spectroscopy, electrochemical impedance spectroscopy (EIS), and Raman spectroscopy. In particular, copper oxide thin films were characterized to understand the change in carrier densities and flat-band potentials.

2. Experimental Details

2.1. Fabrication of Copper Oxide Thin Films

Cu_2O thin films were prepared by electrodeposition on fluorine-doped tin oxide glass substrates (FTO, ~400 nm and 1 cm × 2 cm). The substrates were first cleaned with an ultrasonicator with acetone, isopropyl alcohol (IPA), ethanol, and deionized (DI) water for 5 min and dried in an oven. In this study, all chemicals and reagents were used without further purification. Electrodeposition was performed using a three-electrode system with a potentiostat (SP-150e, BioLogic, Seyssinet-Pariset, France). A cleaned FTO substrate, a coiled platinum wire (0.5 mm diameter), and Ag/AgCl (3 M NaCl) were used as working, counter, and reference electrodes, respectively. Copper sulfate (Sigma-Aldrich, Burlington, MA, USA, >98%) and 3M lactic acid (Sigma-Aldrich, Burlington, MA, USA, >85%) mixed in 40 mL of DI water were used after adjusting pH = 9 with 5 M NaOH. The chronoam-perometric (CA) method was applied at −0.36 V (V vs. Ag/AgCl) for 20 min to deposit Cu_2O thin films on an FTO glass substrate at ~50 °C and with magnetic stirring at 600 rpm. We then carried out thermal oxidation at different temperatures for 1 h on a hot plate using as-prepared Cu_2O thin films after washing with DI water and drying with nitro-gen. After conducting the annealing temperature effects, we found that heterostructured CuO/Cu_2O/FTO and CuO/FTO thin films can be prepared at 350 and 500 °C, respectively (Figure 1). For simplicity, Cu_2O, CuO/Cu_2O, and CuO thin films correspond to Cu_2O/FTO prepared by electrodeposition without annealing, a heterostructured configuration of CuO/Cu_2O/FTO annealed at 350 °C and CuO/FTO annealed at 500 °C.
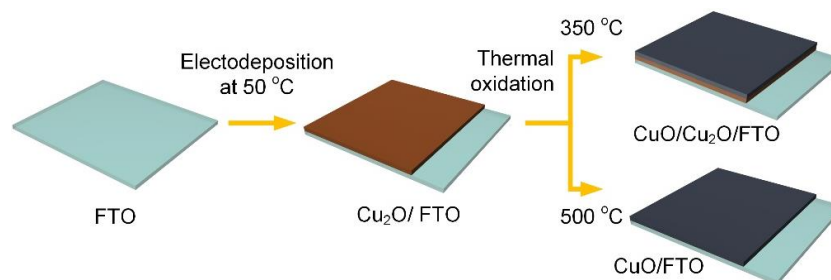
Figure 1. Schematic of the preparation process of copper oxide thin films on an FTO-coated glass substrate using electrodeposition and thermal oxidation at different temperatures.

2.2. Materials Characterization

The surface morphologies of three thin films (Cu_2O, CuO/Cu_2O, and CuO deposited on an FTO-coated glass substrate) were observed by scanning electron microscopy (SEM, Zeiss Gemini 450, Jena, Germany) operated at an acceleration voltage of 10 keV. Ultraviolet-visible spectroscopy (UV-VIS, SEMSO-3000, AUBOTECH, Taipei, Taiwan) was used to examine the optical properties of the thin films. X-ray diffraction (XRD, Brucker D8 DISCOVER, Billerica, MA, USA) with Cu K_α radiation (λ = 0.154184 nm) and Raman microscopy (CL Technology UniDRON-S, New Taipei, Taiwan) with a 532 nm excitation wavelength were applied to investigate the transformation of Cu_2O to CuO. An X-ray photoelectron spectrometer (XPS, Thermo Scientific K-Alpha, Waltham, MA, USA) was used with monochromatic Al K_α radiation and a flood gun to examine the chemical valences of the thin films. All electrochemical measurements were performed using a standard rectangular quartz cuvette of ~20 mL with the three-electrode system. A leakless miniature Ag/AgCl reference electrode (ET072-1, eDAQ, 3.4 M KCl) was used after calibration using the Ag/AgCl (3 M NaCl) reference electrode to convert the potentials to the reversible hydrogen electrode (RHE) scale [51]. While 0.2 M Na_2SO_4 (pH = 6.2) was used as an electrolyte, an active area of thin films of 1.0 cm^2 was set using a chemical-tolerant 3 M tape (Electroplating Tape 470, 3 M). For the Mott–Schottky analysis, the frequency was set at 1k Hz and an amplitude of 10 mV. For PEC measurements, potentials were applied from 0 to 0.5 V (vs. RHE) at the scan rate of 5 mV/s. A solar simulator with an AM 1.5 G filter (Enlitech SS-X, Enlitech, Kaohsiung, Taiwan) and a light intensity of 100 mW/cm^2 was used as a light source after accurate calibration. The EIS was also adopted to ensure the rate of charge-transfer reactions between the electrode surface and the electrolyte. The Nyquist plots were obtained by applying a static potential of 0.3 V vs. Ag/AgCl with the 5 mV sinusoidal wave from 0.1 to 1 M Hz without and with light illumination.

3. Results and Discussion

3.1. Morphology and Optical Properties of Copper Oxide Thin Films

The surface morphologies of the thin films were examined by SEM and AFM, as shown in Figure 2. After 1-h thermal treatment at 350 and 500 °C, it was observed that the grain sizes and shapes changed, and the surfaces became denser than pristine Cu_2O thin films. The cross-sectional view of the Cu_2O thin film indicates a thickness of ~1.40 μm. Due to the difference in density (Cu_2O: 6.0 g/cm^3 and CuO: 6.31 g/cm^3) [52] and the thermal expansion of Cu_2O [53] after thermal oxidation ($Cu_2O + 1/2O_2 \rightarrow 2CuO$), a slight increase in thickness was observed, similar to previous reports [28]. As summarized in Table S3, energy-dispersive X-ray spectroscopy (EDS) was also employed to examine the chemical composition of the thin films before and after annealing at 350 and 500 °C. It verifies the successful fabrication of Cu_2O using electrodeposition and the complete transformation of Cu_2O to CuO after annealing at 500 °C for 1 h. Additionally, the EDS analysis shows a heterostructure of CuO/Cu_2O ([Cu]/[O] = 1.52). The SEM analysis illustrates that the annealing of metal oxides [54] led to the agglomeration of adjacent grains [55].
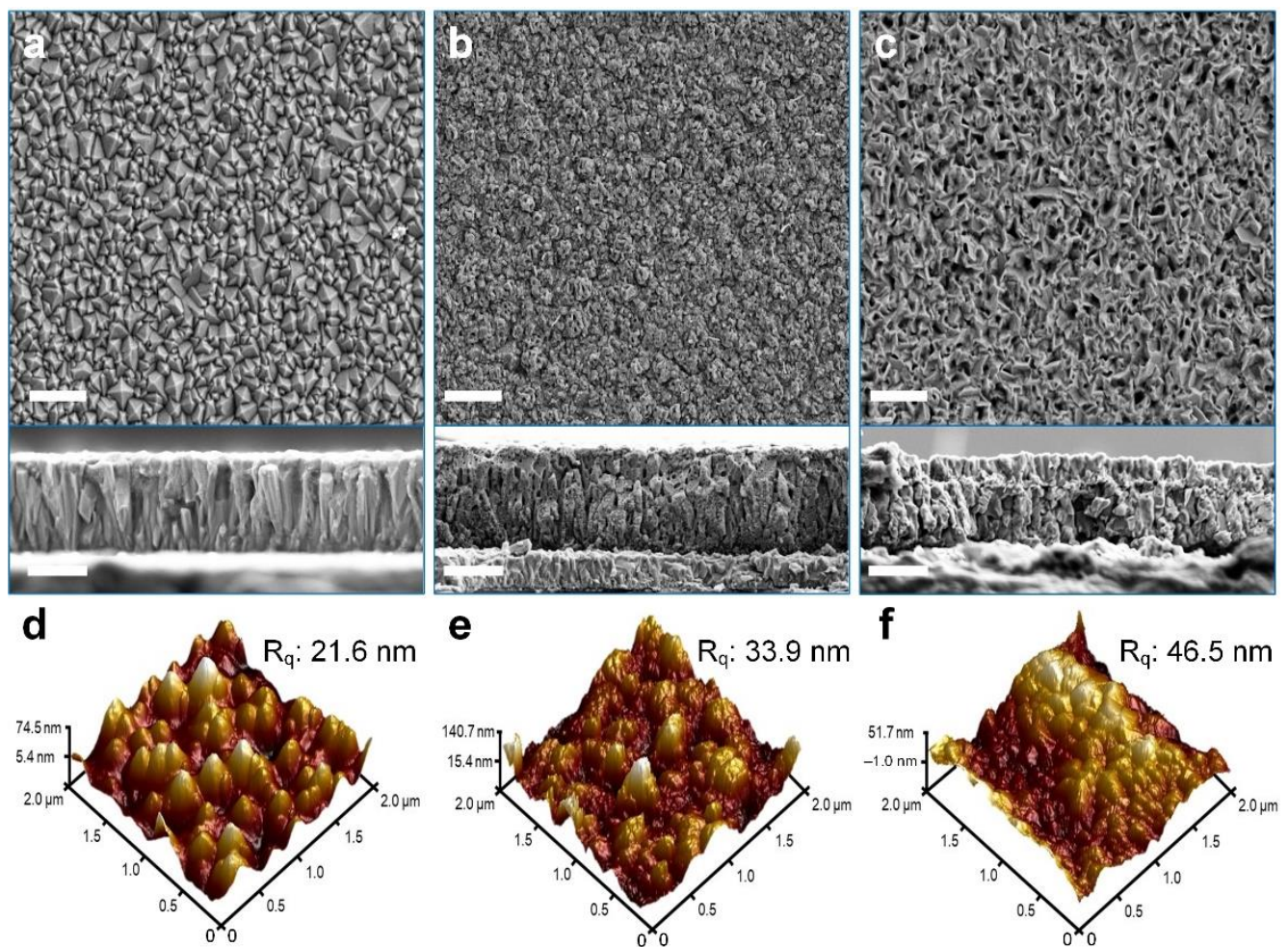
Figure 2. Typical top and cross-sectional views of SEM images for (**a**) Cu$_2$O, (**b**) CuO/Cu$_2$O, and (**c**) CuO thin films. Scale bar = 1 µm. Corresponding AFM images of the thin films, (**d**), (**e**), and (**f**), respectively, obtained with the tapping mode. R$_q$ denotes RMS roughness. Image areas are 2 µm × 2 µm.

A similar trend was also observed using AFM (Figure 2d–f), which is attributed to the random distribution of grains and phase changes [56]. It was found that the root mean square (RMS) roughness of the thin films increased from 21.6 nm (Cu$_2$O) to 33.9 nm (CuO/Cu$_2$O at 350 °C) and 46.5 nm (CuO at 500 °C) (Cu$_2$O < CuO/Cu$_2$O < CuO). We assume that the controlling of thin film thicknesses using the electrolyte temperature affects RMS roughness [40]. Furthermore, since the light absorption properties of thin films play an essential role in PEC performance, we measured the absorbance of Cu$_2$O, CuO/Cu$_2$O, and CuO thin films using a UV-Vis spectrometer. Figure 3a shows the typical absorbance of the three thin films, demonstrating that the Cu$_2$O thin film has an absorption edge in the range of 500 to 650 nm. It shows that the absorption edge of thermally treated thin films (CuO/Cu$_2$O and CuO) was red-shifted. In addition, we measured the band gaps of these samples using the Tauc plot analysis [57] using $(\alpha h\nu)^n = B(h\nu - E_g)$, where α is the absorption coefficient, h is the Plank constant, ν is the photon energy, B is a constant, and E_g is the band gap. The copper oxide thin films were analyzed with a direct transition ($n = 2$). As Figure 3b and Table S4 show, the band gaps measured (Cu$_2$O: 2.35 eV, CuO/Cu$_2$O: 1.81 eV, CuO: 1.45 eV) are in good agreement with a previous study [28]. CuO/Cu$_2$O and CuO exhibited a higher band gap than Cu$_2$O, denoting that they can expand the absorption range of visible light compared to Cu$_2$O. Consequently, it could improve PEC performance [58].
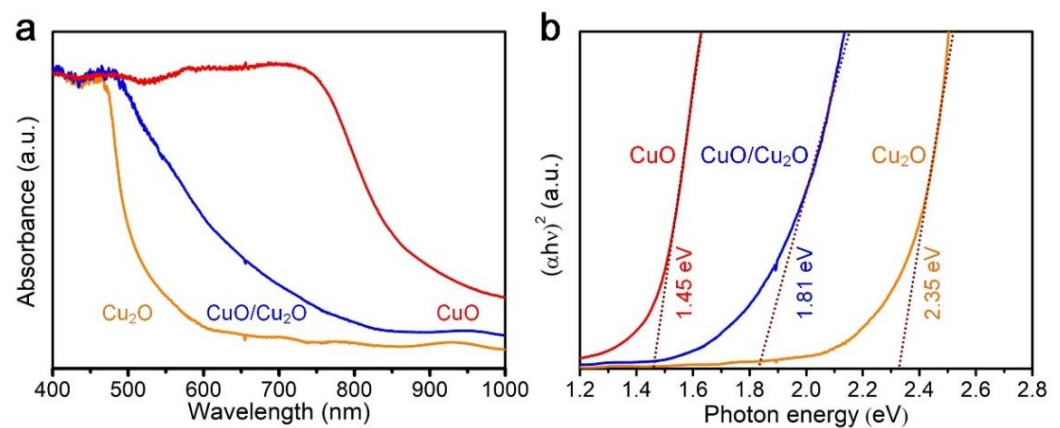
Figure 3. (**a**) Normalized absorbance spectra and (**b**) Tauc plots of Cu_2O, CuO/Cu_2O, and CuO thin films.

3.2. Characterization of Copper Oxide Thin Films Using XRD, Raman Spectroscopy, and XPS

Figure 4a demonstrates the XRD pattern for the CuO/Cu_2O thin film, while Figure S1 shows those for Cu_2O and CuO thin films. For the Cu_2O thin film, the peaks at 36.6° and 42.5° are attributed to the (111) and (200) planes [59,60] (JCPDS file No. 99-0041). The XRD pattern of Cu_2O illustrates that the thin films exhibit the (200) plane as the preferential growth direction [61]. Cu_2O and CuO diffraction peaks were observed in the thin film annealed at 350 °C, while the thin film annealed at 500 °C exhibited the pure CuO phase (JCPDS file No. 72-0269) [62]. The distinctive diffraction peak at 35.6° indicates that the thin film has a good crystal structure of CuO after annealing at 500 °C. The XRD analysis may support that the thermal oxidation process at 350 °C produced heterostructured CuO/Cu_2O similar to the previous studies [28,63]. The particle sizes of the thin films were evaluated using the Scherrer–Debye equation [64], $D = \frac{K\lambda}{\beta \cos\theta}$, where D is the average crystal particle size, K is a constant, λ is the wavelength of X-ray, β is the full width at half maximum (FWHM), and θ is the Bragg angle. The Cu_2O and CuO thin films were determined as 22.3 and 29.1 nm, respectively, indicating the improvement of the homogeneity of the thin films and the enhancement of the electrical properties [65]. As shown in Figure 4b, we also performed Raman spectroscopic measurements in the spectral region of 100 to 800 cm^{-1} to complement the XRD and SEM analyses. Single-phase Cu_2O has only one Raman active mode (F_{2g}), while single-phase CuO has three Raman active modes ($A_g + 2B_g$) [66]. The Raman bands of the Cu_2O thin film at 218, 278, and 623 cm^{-1} are contributed from the second-order Raman-allowed modes of single-phase Cu_2O [67], while those of the CuO thin film at 287, 338, and 614 cm^{-1} are in good agreement with single-phase CuO, as reported in the literature [68]. As the annealing temperatures increased, Cu_2O peaks decreased, and CuO peaks appeared gradually. The Raman spectrum of the CuO/Cu_2O thin film shows that the combined peaks of Cu_2O and CuO (209, 279, 329, and 614 cm^{-1}) are assigned to the A_g and B_g modes [66]. As illustrated in Figure 4c,d, XPS was also used to analyze the elemental compositions of copper oxides. Figure 4c shows a representative XPS survey spectrum of the CuO/Cu_2O thin film [69]. All XPS spectra were calibrated with the C 1s photoemission peak of adventitious carbon at 284.5 eV [70]. Figure S2a,b shows the XPS spectra of Cu 2p of the Cu_2O and CuO thin films that align with those reported in the literature [71,72]. To examine the heterostructure of the CuO/Cu_2O thin film, we carried out the deconvolution of its XPS spectrum using XPSPEAK 4.1. Two main peaks and satellite peaks were observed in the spectrum. The deconvolution process identified that the peaks at 932.91 and 952.74 eV are related to Cu^+ (Cu_2O), which are assigned to Cu $2p_{3/2}$ and Cu $2p_{1/2}$. By contrast, those at 934.27 and 954.12 eV are attributed to Cu $2p_{3/2}$ and Cu $2p_{1/2}$, confirming the presence of Cu^{2+} (CuO). As summarized in Figure S2c, we observed a slightly broadened peak for Cu $2p_{3/2}$ of CuO/Cu_2O compared to CuO. Based on the deconvolution of the CuO/Cu_2O thin film, we manifested that the sample is a

heterojunction ($CuO:Cu_2O$ = 56.4%:43.6%), which qualitatively agrees with the analysis using SEM/EDS (Table S3). As reported [73,74], metal oxide thin films fabricated via simple annealing could generate cracks inside thin films due to thermal stress, enabling X-ray beams to irradiate the FTO surface. Thus, the peak at 496.08 eV can be assigned to Sn 3d originating from FTO [75]. We assumed that the CuO/Cu_2O thin film prepared by electrodeposition could become a heterojunction configuration as reported [28] according to the characterization of the SEM/EDS, XRD, XPS, and Raman spectroscopic analyses.
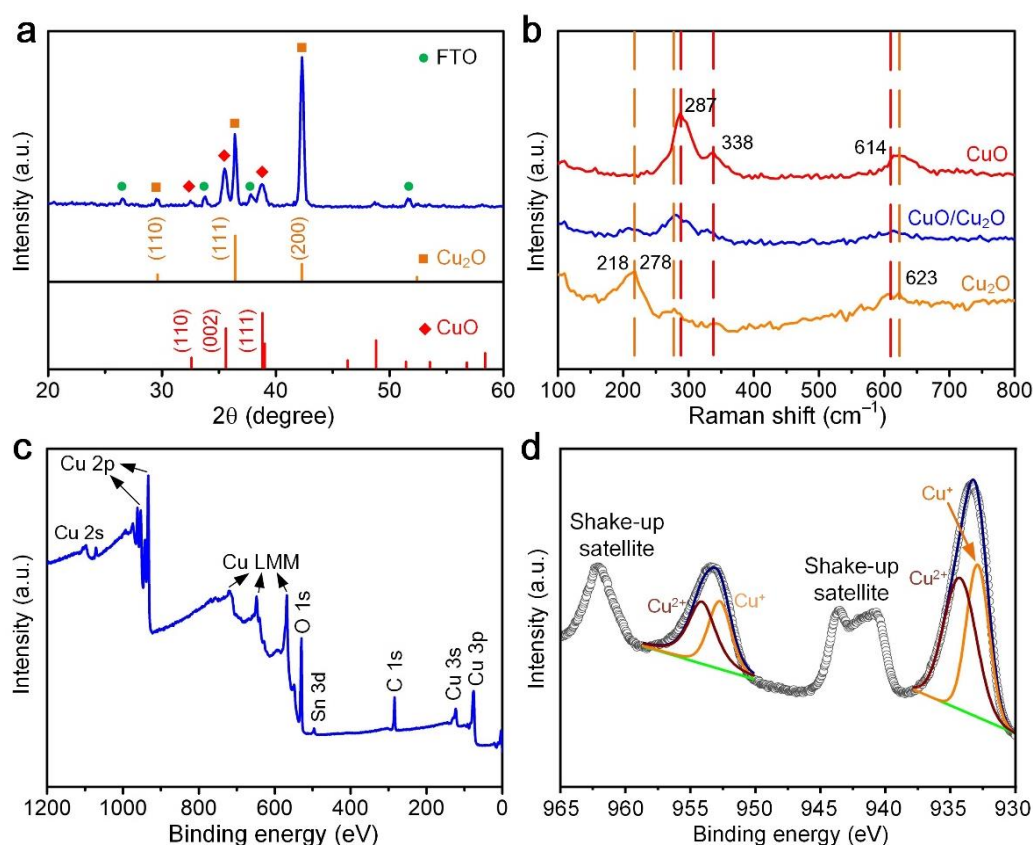

Figure 4. (**a**) XRD pattern of the CuO/Cu_2O thin film. The diffraction peaks can be indexed with Cu_2O (JCPDS file No. 99-0041) and CuO (JCPDS file No. 72-0269); (**b**) Raman spectra of Cu_2O, CuO/Cu_2O, and CuO thin films; (**c**) the full XPS survey spectrum of the CuO/Cu_2O thin film; (**d**) high-resolution XPS spectrum of Cu 2p of the CuO/Cu_2O thin film. The dotted curve is the experimental data, while solid curves are after the curve-fitting procedure.

3.3. Electrochemical Measurements of Copper Oxide Thin Films

The Mott–Schottky technique was applied to examine changes in electrochemical interfaces between the electrolyte and photocathodes prepared in this study. Carrier densities and flat band potentials can be accurately measured using the Mott–Schottky equation for p-type semiconductors [76,77].

$$\frac{1}{C^2} = -\frac{2}{\varepsilon\varepsilon_0 e N_A A^2}\left(V - V_{fb} - \frac{k_B T}{e}\right)$$

where C is the interfacial capacitance, ε is the dielectric constant of the semiconductor electrode, ε_0 is the vacuum permittivity, e is the electron charge, V_{fb} is the flat band potential, N_A is the major carrier density, A is the electrode area, V is the applied voltage, k_B is the Boltzmann constant, and T is the absolute temperature. Carrier densities of p-type copper oxides (N_A) can be determined from a straight line by plotting $1/C^2$ vs. V, while the flat band potential (V_{fb}) can be obtained from the intercept with the x-axis. While carrier

densities affect charge transfer rates [28,78,79], the flat band potential is associated with a driving force to separate electron-hole pairs in the space charge region, which can be used as one of the key factors to predict PEC performance. For example, a shift of the flat band to a more positive potential denotes improved electron transfer, decreasing the recombination of electron-hole pairs and boosting PEC efficiencies [80]. Figure 5a–c demonstrates Mott–Schottky plots for Cu_2O, CuO/Cu_2O, and CuO thin films. The three thin films exhibit p-type semiconductor characteristics with a negative slope. ε of 7.6 for Cu_2O [81] and 10.26 [36] for CuO/Cu_2O and CuO thin films were used to calculate carrier densities. It resulted in a N_A value of 1.79×10^{16}, 6.91×10^{17}, and 6.26×10^{17} cm^{-3}, respectively, in the order of $Cu_2O < CuO < CuO/Cu_2O$. Moreover, we also successfully confirmed the same trend of flat band potentials of 0.46, 1.04, and 0.89 V, respectively. According to the Mott–Schottky analysis, the improved PEC performance of the heterojunction structure of CuO/Cu_2O can be rationally anticipated [28]. Figure 5d,e shows Nyquist plots of three thin films without and with illumination. It exhibited that the radius of the semicircle decreased with light illumination to the working electrode. It denotes that illumination accelerated the rate of the charge transfer reaction between the photoelectrode surface and the electrolyte, and accordingly, the carrier density increased. As shown in Figure 5e, EIS data were then analyzed by fitting with an equivalent electrical circuit model to examine transfer resistance on different photoelectrode materials. As reported, R_s is the series resistance, R_{sc} is the resistance on the depletion layer, and R_{ct} is the charge transfer resistance, while C_{sc} is the capacitance related to the depletion layer of a semiconductor and C_H is the Helmholtz layer capacitance [82]. It is anticipated that the heterostructured electrode exhibits the lowest charge transfer resistance (R_{ct}) due to its smallest diameter, leading to the highest charge transfer reaction rate [28]. Figure 5f illustrates representative photocurrent densities of three electrode materials under AM1.5G illumination. For the Cu_2O thin film, a photocurrent of 0.08 mA/cm^2 at 0 V (vs. RHE) was observed, while for the CuO/Cu_2O and CuO thin films, the photocurrent increased to 1.03 and 0.92 mA/cm^2, respectively. It aligns with Mott–Schottky and EIS-based analyses. Table 1 compiles carrier densities, flat band potentials, and photocurrent densities of Cu_2O, CuO/Cu_2O, and CuO thin films. It is noted that PEC performance can be affected by too high annealing temperatures, altering the electrical property of FTO-based thin films [83]. In summary, it manifests that a higher carrier density, a higher flat band potential, and lower charge transfer resistance of the heterojunction CuO/Cu_2O thin film could be highly correlated with the PEC performance compared to the Cu_2O and CuO thin films [28].

Table 1. Experimental values of carrier density (N_A), flat band potential (V_{fb}), and photocurrent density for p-type Cu_2O, CuO/Cu_2O, and CuO thin films.

Thin Film	N_A (cm^{-3})	V_{fb} (V)	Photocurrent Density (mA/cm^2)
Cu_2O	1.79×10^{16}	0.46	0.08
CuO/Cu_2O	6.91×10^{17}	1.04	1.03
CuO	6.26×10^{17}	0.89	0.92

Figure 5. Mott–Schottky plots of (**a**) Cu_2O, (**b**) CuO/Cu_2O, and (**c**) CuO thin films and Nyquist plots of Cu_2O, CuO/Cu_2O, and CuO thin films without (**d**) and with (**e**) light illumination; (**f**) comparison of photocurrent densities of the three thin films.

4. Conclusions

Cu_2O thin films were effectively fabricated using electrodeposition, followed by controlling annealing temperatures. The thickness and morphology of thin films were analyzed using SEM, while the surface roughness was investigated using AFM. XRD, XPS, and Raman spectroscopic measurements confirmed the heterojunction structure of CuO/Cu_2O after annealing at 350 °C. As the thermal oxidation temperatures increased, the light absorbance edge of the thin films was red-shifted, demonstrating a better absorber in the visible region and enhancing photocurrent densities in the order of Cu_2O < CuO < CuO/Cu_2O. In particular, the Mott–Schottky and EIS measurements confirmed that the heterojunction structure has a higher carrier concentration, a larger flat band potential, and a lower charge transfer resistance than the Cu_2O and CuO thin films. Accordingly, the CuO/Cu_2O thin film annealed at 350 °C achieved a boosted photocurrent density of 1.03 mA/cm^2 at 0 V (vs. RHE). We demonstrated that the heterojunction configuration of copper oxide thin films (CuO/Cu_2O) via the cost-effective electrodeposition method could improve PEC performance by reducing the electro-hole pair recombination and increasing carrier densities.

Supplementary Materials: The following supporting information can be downloaded at: https://www.mdpi.com/article/10.3390/coatings12121839/s1, Table S1: Compilation of copper oxide-based photocathodes used for PEC water splitting, Table S2: Compilation of heterostructured copper oxide-based photoelectrodes, Table S3: EDS analysis results of Cu_2O, CuO/Cu_2O, and CuO thin films, Table S4: Band gaps of Cu_2O, CuO/Cu_2O, and CuO thin films, Table S5: EIS parameters obtained by fitting the Nyquist plots with the equivalent circuit, Figure S1: XRD patterns of (a) Cu_2O, (b) CuO/Cu_2O, and (c) CuO thin films, Figure S2: XPS spectra for Cu 2p of (a) Cu_2O and (b) CuO thin films and (c) comparison of CuO and CuO/Cu_2O thin films.

Author Contributions: Conceptualization, Y.C.; data curation, T.-H.Y. and B.-J.L.; investigation, T.-H.Y., B.-J.L., Y.-W.L., Y.-S.L. and C.-W.L.; methodology, T.-H.Y. and B.-J.L.; project administration, C.C., H.-C.C. and Y.C.; software, T.-H.Y.; supervision, Y.C.; visualization, T.-H.Y., B.-J.L. and Y.-W.L.; writing original draft preparation, T.-H.Y., B.-J.L., Y.-W.L. and Y.-S.L.; writing—review and editing, Y.-P.L., C.C., H.-C.C. and Y.C. All authors have read and agreed to the published version of the manuscript.

Institutional Review Board Statement: Not applicable.

Informed Consent Statement: Not applicable.

Data Availability Statement: Not applicable.

Conflicts of Interest: The authors declare no conflict of interest.

References

1. van Ruijven, B.J.; De Cian, E.; Wing, I.S. Amplification of future energy demand growth due to climate change. *Nat. Commun.* **2019**, *10*, 2762. [CrossRef]
2. Abdin, Z.; Alim, M.A.; Saidur, R.; Islam, M.R.; Rashmi, W.; Mekhilef, S.; Wadi, A. Solar energy harvesting with the application of nanotechnology. *Renew. Sust. Energ. Rev.* **2013**, *26*, 837–852. [CrossRef]
3. Guo, C.X.; Guai, G.H.; Li, C.M. Graphene based materials: Enhancing solar energy harvesting. *Adv. Energy Mater.* **2011**, *1*, 448–452. [CrossRef]
4. Chang, S.-Y.; Cheng, P.; Li, G.; Yang, Y. Transparent polymer photovoltaics for solar energy harvesting and beyond. *Joule* **2018**, *2*, 1039–1054. [CrossRef]
5. Minggu, L.J.; Daud, W.R.W.; Kassim, M.B. An overview of photocells and photoreactors for photoelectrochemical water splitting. *Int. J. Hydrog. Energy* **2010**, *35*, 5233–5244. [CrossRef]
6. Ahmad, H.; Kamarudin, S.K.; Minggu, L.J.; Kassim, M. Hydrogen from photo-catalytic water splitting process: A review. *Renew. Sust. Energ. Rev.* **2015**, *43*, 599–610. [CrossRef]
7. Lin, H.; Huang, C.P.; Li, W.; Ni, C.; Shah, S.I.; Tseng, Y.-H. Size dependency of nanocrystalline TiO_2 on its optical property and photocatalytic reactivity exemplified by 2-chlorophenol. *Appl. Catal. B* **2006**, *68*, 1–11. [CrossRef]
8. Yamada, Y.; Kanemitsu, Y. Determination of electron and hole lifetimes of rutile and anatase TiO_2 single crystals. *Appl. Phys. Lett.* **2012**, *101*, 133907. [CrossRef]
9. Xie, Y.; Ju, Y.; Toku, Y.; Morita, Y. Synthesis of a single-crystal Fe_2O_3 nanowire array based on stress-induced atomic diffusion used for solar water splitting. *R. Soc. Open Sci.* **2018**, *5*, 172126. [CrossRef]
10. Sharma, P.; Jang, J.-W.; Lee, J.S. Key strategies to advance the photoelectrochemical water splitting performance of α-Fe_2O_3 photoanode. *ChemCatChem* **2019**, *11*, 157–179. [CrossRef]
11. Sharp, I.D.; Cooper, J.K.; Toma, F.M.; Buonsanti, R. Bismuth vanadate as a platform for accelerating discovery and development of complex transition-metal oxide photoanodes. *ACS Energy Lett.* **2017**, *2*, 139–150. [CrossRef]
12. Butler, K.T.; Dringoli, B.J.; Zhou, L.; Rao, P.M.; Walsh, A.; Titova, L.V. Ultrafast carrier dynamics in $BiVO_4$ thin film photoanode material: Interplay between free carriers, trapped carriers and low-frequency lattice vibrations. *J. Mater. Chem.* **2016**, *4*, 18516–18523. [CrossRef]
13. Bocarsly, A.B.; Bookbinder, D.C.; Dominey, R.N.; Lewis, N.S.; Wrighton, M.S. Photoreduction at illuminated p-type semiconducting silicon photoelectrodes. Evidence for Fermi level pinning. *J. Am. Chem. Soc.* **1980**, *102*, 3683–3688. [CrossRef]
14. Luo, Z.; Wang, T.; Gong, J. Single-crystal silicon-based electrodes for unbiased solar water splitting: Current status and prospects. *Chem. Soc. Rev.* **2019**, *48*, 2158–2181. [CrossRef] [PubMed]
15. Jin, Z.; Hu, Z.; Jimmy, C.Y.; Wang, J. Room temperature synthesis of a highly active Cu/Cu_2O photocathode for photoelectrochemical water splitting. *J. Mater. Chem. A* **2016**, *4*, 13736–13741. [CrossRef]

16. Kim, D.S.; Kim, Y.B.; Choi, J.H.; Suh, H.W.; Lee, H.H.; Lee, K.W.; Jung, S.H.; Kim, J.J.; Deshpande, N.G.; Cho, H.K. Toward simultaneous achievement of outstanding durability and photoelectrochemical reaction in Cu_2O photocathodes via electrochemically designed resistive switching. *Adv. Energy Mater.* **2021**, *11*, 2101905. [CrossRef]

17. Wang, Z.; Zhang, L.; Schülli, T.U.; Bai, Y.; Monny, S.A.; Du, A.; Wang, L. Identifying copper vacancies and their role in the CuO based photocathode for water splitting. *Angew. Chem.* **2019**, *131*, 17768–17773. [CrossRef]

18. Li, J.; Jin, X.; Li, R.; Zhao, Y.; Wang, X.; Liu, X.; Jiao, H. Copper oxide nanowires for efficient photoelectrochemical water splitting. *Appl. Catal. B* **2019**, *240*, 1–8. [CrossRef]

19. Paracchino, A.; Laporte, V.; Sivula, K.; Grätzel, M.; Thimsen, E. Highly active oxide photocathode for photoelectrochemical water reduction. *Nat. Mater.* **2011**, *10*, 456–461. [CrossRef]

20. Paracchino, A.; Brauer, J.C.; Moser, J.-E.; Thimsen, E.; Graetzel, M. Synthesis and characterization of high-photoactivity electrodeposited Cu_2O solar absorber by photoelectrochemistry and ultrafast spectroscopy. *J. Phys. Chem. C* **2012**, *116*, 7341–7350. [CrossRef]

21. Zhang, Z.; Dua, R.; Zhang, L.; Zhu, H.; Zhang, H.; Wang, P. Carbon-layer-protected cuprous oxide nanowire arrays for efficient water reduction. *ACS Nano* **2013**, *7*, 1709–1717. [CrossRef]

22. Guo, X.; Diao, P.; Xu, D.; Huang, S.; Yang, Y.; Jin, T.; Wu, Q.; Xiang, M.; Zhang, M. CuO/Pd composite photocathodes for photoelectrochemical hydrogen evolution reaction. *Int. J. Hydrog. Energy.* **2014**, *39*, 7686–7696. [CrossRef]

23. Chiang, C.-Y.; Chang, M.-H.; Liu, H.-S.; Tai, C.Y.; Ehrman, S. Process intensification in the production of photocatalysts for solar hydrogen generation. *Ind. Eng. Chem. Res.* **2012**, *51*, 5207–5215. [CrossRef]

24. Wijesundera, R.P. Fabrication of the CuO/Cu_2O heterojunction using an electrodeposition technique for solar cell applications. *Semicond. Sci. Technol.* **2010**, *25*, 045015. [CrossRef]

25. Matsumura, H.; Fujii, A.F.A.; Kitatani, T.K.T. Properties of high-mobility Cu_2O films prepared by thermal oxidation of Cu at low temperatures. *Jpn. J. Appl. Phys.* **1996**, *35*, 5631. [CrossRef]

26. Xing, H.; E, L.; Guo, Z.; Zhao, D.; Liu, Z. Enhancement in the charge transport and photocorrosion stability of CuO photocathode: The synergistic effect of spatially separated dual-cocatalysts and p-n heterojunction. *Chem. Eng. J.* **2020**, *394*, 124907. [CrossRef]

27. Jian, J.; Kumar, R.; Sun, J. Cu_2O/ZnO p–n junction decorated with NiO_x as a protective layer and cocatalyst for enhanced photoelectrochemical water splitting. *ACS Appl. Energy Mater.* **2020**, *3*, 10408–10414. [CrossRef]

28. Yang, Y.; Xu, D.; Wu, Q.; Diao, P. Cu_2O/CuO bilayered composite as a high-efficiency photocathode for photoelectrochemical hydrogen evolution reaction. *Sci. Rep.* **2016**, *6*, 35158. [CrossRef]

29. Bae, H.; Burungale, V.; Na, W.; Rho, H.; Kang, S.H.; Ryu, S.-W.; Ha, J.-S. Nanostructured CuO with a thin g-C_3N_4 layer as a highly efficient photocathode for solar water splitting. *RSC Adv.* **2021**, *11*, 16083–16089. [CrossRef]

30. Mary, A.S.; Murugan, C.; Pandikumar, A. Uplifting the charge carrier separation and migration in Co-doped $CuBi_2O_4/TiO_2$ pn heterojunction photocathode for enhanced photoelectrocatalytic water splitting. *J. Colloid Interface Sci.* **2022**, *608*, 2482–2492. [CrossRef]

31. Baek, S.K.; Kim, J.S.; Yun, Y.D.; Kim, Y.B.; Cho, H.K. Cuprous/cupric heterojunction photocathodes with optimal phase transition interface via preferred orientation and precise oxidation. *ACS Sustain. Chem. Eng.* **2018**, *6*, 10364–10373. [CrossRef]

32. Ma, M.; Lei, E.; Zhao, D.; Xin, Y.; Wu, X.; Meng, Y.; Liu, Z. The p-n heterojunction of $BiVO_4/Cu_2O$ was decorated by plasma Ag NPs for efficient photoelectrochemical degradation of Rhodamine B. *Colloids Surf. A Physicochem. Eng. Asp.* **2022**, *633*, 127834. [CrossRef]

33. Hossain, R.; Nekouei, R.K.; Al Mahmood, A.; Sahajwalla, V. Value-added fabrication of NiO-doped CuO nanoflakes from waste flexible printed circuit board for advanced photocatalytic application. *Sci. Rep.* **2022**, *12*, 12171. [CrossRef] [PubMed]

34. Chen, Y.-C.; Dong, P.-H.; Hsu, Y.-K. Defective indium tin oxide forms an ohmic back contact to an n-type Cu_2O photoanode to accelerate charge-transfer kinetics for enhanced low-bias photoelectrochemical water splitting. *ACS Appl. Mater. Interfaces* **2021**, *13*, 38375–38383. [CrossRef] [PubMed]

35. Zhong, X.; Song, Y.; Cui, A.; Mu, X.; Li, L.; Han, L.; Shan, G.; Liu, H. Adenine-functionalized graphene oxide as a charge transfer layer to enhance activity and stability of Cu_2O photocathode for CO_2 reduction reaction. *Appl. Surf. Sci.* **2022**, *591*, 153197. [CrossRef]

36. Chiang, C.-Y.; Aroh, K.; Franson, N.; Satsangi, V.R.; Dass, S.; Ehrman, S. Copper oxide nanoparticle made by flame spray pyrolysis for photoelectrochemical water splitting—Part II. Photoelectrochemical study. *Int. J. Hydrog. Energy* **2011**, *36*, 15519–15526. [CrossRef]

37. Kalanur, S.S.; Lee, Y.J.; Seo, H. Enhanced and stable photoelectrochemical H_2 production using a engineered nano multijunction with Cu_2O photocathode. *Mater. Today Chem.* **2022**, *26*, 101031. [CrossRef]

38. Du, F.; Chen, Q.-Y.; Wang, Y.-H. Effect of annealing process on the heterostructure CuO/Cu_2O as a highly efficient photocathode for photoelectrochemical water reduction. *J. Phys. Chem. Solids* **2017**, *104*, 139–144. [CrossRef]

39. Jamali, S.; Moshaii, A.; Mohammadian, N. Improvement of photoelectrochemical and stability properties of electrodeposited Cu_2O thin films by annealing processes. *Phys. Status Solidi. A* **2017**, *214*, 1700380. [CrossRef]

40. Chang, C.-J.; Lai, C.-W.; Jiang, W.-C.; Li, Y.-S.; Choi, C.; Yu, H.-C.; Chen, S.-J.; Choi, Y. Fabrication and characterization of P-type semiconducting copper oxide-based thin-film photoelectrodes for solar water splitting. *Coatings* **2022**, *12*, 1206. [CrossRef]

41. Kyesmen, P.I.; Nombona, N.; Diale, M. Heterojunction of nanostructured α-Fe_2O_3/CuO for enhancement of photoelectrochemical water splitting. *J. Alloys Compd.* **2021**, *863*, 158724.

42. Ma, J.; Wang, Q.; Li, L.; Zong, X.; Sun, H.; Tao, R.; Fan, X. Fe$_2$O$_3$ nanorods/CuO nanoparticles pn heterojunction photoanode: Effective charge separation and enhanced photoelectrochemical properties. *J. Colloid Interface Sci.* **2021**, *602*, 32–42. [CrossRef] [PubMed]

43. Liu, C.; Meng, F.; Zhang, L.; Zhang, D.; Wei, S.; Qi, K.; Fan, J.; Zhang, H.; Cui, X. CuO/ZnO heterojunction nanoarrays for enhanced photoelectrochemical water oxidation. *Appl. Surf. Sci.* **2019**, *469*, 276–282. [CrossRef]

44. Jabeen, S.; Sherazi, T.A.; Ullah, R.; Naqvi, S.A.R.; Rasheed, M.A.; Ali, G.; Shah, A.U.; Khan, Y. Electrodeposition-assisted formation of anodized TiO$_2$–CuO heterjunctions for solar water splitting. *Appl. Nanosci.* **2021**, *11*, 79–90. [CrossRef]

45. Zhang, J.; Ma, H.; Liu, Z. Highly efficient photocatalyst based on all oxides WO$_3$/Cu$_2$O heterojunction for photoelectrochemical water splitting. *Appl. Catal. B* **2017**, *201*, 84–91. [CrossRef]

46. Alizadeh, M.; Tong, G.B.; Qadir, K.W.; Mehmood, M.S.; Rasuli, R. Cu$_2$O/InGaN heterojunction thin films with enhanced photoelectrochemical activity for solar water splitting. *Renew. Energy* **2020**, *156*, 602–609. [CrossRef]

47. Zhang, S.; Yan, J.; Yang, S.; Xu, Y.; Cai, X.; Li, X.; Zhang, X.; Peng, F.; Fang, Y. Electrodeposition of Cu$_2$O/g-C$_3$N$_4$ heterojunction film on an FTO substrate for enhancing visible light photoelectrochemical water splitting. *Chin. J. Catal.* **2017**, *38*, 365–371. [CrossRef]

48. De Jongh, P.E.; Vanmaekelbergh, D.; Kelly, J.J. Cu$_2$O: Electrodeposition and characterization. *Chem. Mater.* **1999**, *11*, 3512–3517. [CrossRef]

49. Jiao, X.; Chen, Z.; Li, X.; Sun, Y.; Gao, S.; Yan, W.; Wang, C.; Zhang, Q.; Lin, Y.; Luo, Y.; et al. Defect-mediated electron–hole separation in one-unit-cell ZnIn$_2$S$_4$ layers for boosted solar-driven CO$_2$ reduction. *J. Am. Chem. Soc.* **2017**, *139*, 7586–7594. [CrossRef]

50. Di, J.; Xia, J.; Chisholm, M.F.; Zhong, J.; Chen, C.; Cao, X.; Dong, F.; Chi, Z.; Chen, H.; Weng, Y.-X.; et al. Defect-tailoring mediated electron–hole separation in single-unit-cell Bi$_3$O$_4$Br nanosheets for boosting photocatalytic hydrogen evolution and nitrogen fixation. *Adv. Mater.* **2019**, *31*, 1807576. [CrossRef]

51. Wang, L.; Lee, C.-Y.; Schmuki, P. Solar water splitting: Preserving the beneficial small feature size in porous α-Fe$_2$O$_3$ photoelectrodes during annealing. *J. Mater. Chem. A* **2013**, *1*, 212–215. [CrossRef]

52. Jayathilaka, C.; Kapaklis, V.; Siripala, W.; Jayanetti, S. Improved efficiency of electrodeposited p-CuO/n-Cu$_2$O heterojunction solar cell. *Appl. Phys. Express.* **2015**, *8*, 065503. [CrossRef]

53. De Los Santos Valladares, L.; Salinas, D.H.; Dominguez, A.B.; Najarro, D.A.; Khondaker, S.I.; Mitrelias, T.; Barnes, C.H.W.; Aguiar, J.A.; Majima, Y. Crystallization and electrical resistivity of Cu$_2$O and CuO obtained by thermal oxidation of Cu thin films on SiO$_2$/Si substrates. *Thin Solid Film* **2012**, *520*, 6368–6374. [CrossRef]

54. Eskandari, A.; Sangpour, P.; Vaezi, M.R. Hydrophilic Cu$_2$O nanostructured thin films prepared by facile spin coating method: Investigation of surface energy and roughness. *Mater. Chem. Phys.* **2014**, *147*, 1204–1209. [CrossRef]

55. Masudy-Panah, S.; Moakhar, R.S.; Chua, C.S.; Kushwaha, A.; Wong, T.I.; Dalapati, G.K. Rapid thermal annealing assisted stability and efficiency enhancement in a sputter deposited CuO photocathode. *RSC Adv.* **2016**, *6*, 29383–29390. [CrossRef]

56. Raship, N.A.; Sahdan, M.Z.; Adriyanto, F.; Nurfazliana, M.F.; Bakri, A.S. Effect of annealing temperature on the properties of copper oxide films prepared by dip coating technique. *AIP Conf. Proc.* **2017**, *1788*, 030121.

57. Makuła, P.; Pacia, M.; Macyk, W. How to correctly determine the band gap energy of modified semiconductor photocatalysts based on UV—Vis spectra. *J. Phys. Chem. Lett.* **2018**, *9*, 6814–6817. [CrossRef]

58. Ju, S.; Kang, H.; Jun, J.; Son, S.; Park, J.; Kim, W.; Lee, H. Periodic micropillar-patterned FTO/BiVO$_4$ with superior light absorption and separation efficiency for efficient PEC performance. *Small* **2021**, *17*, 2006558. [CrossRef] [PubMed]

59. Zhang, H.; Yu, Y.; Shen, X.; Hu, X. A Cu$_2$O/Cu/carbon cloth as a binder-free electrode for non-enzymatic glucose sensors with high performance. *New J. Chem.* **2020**, *44*, 1993–2000. [CrossRef]

60. Wang, Y.; Steigert, A.; Yin, G.; Parvan, V.; Klenk, R.; Schlatmann, R.; Lauermann, I. Cu$_2$O as a potential intermediate transparent conducting oxide layer for monolithic perovskite-CIGSe tandem solar cells. *Phys. Status Solidi C* **2017**, *14*, 1700164.

61. Fentahun, D.A.; Tyagi, A.; Singh, S.; Sinha, P.; Mishra, A.; Danayak, S.; Kumar, R.; Kar, K.K. Tunable optical and electrical properties of p-type Cu$_2$O thin films. *J. Mater. Sci. Mater.* **2021**, *32*, 11158–11172. [CrossRef]

62. Kshirsagar, J.M.; Shrivastava, R.; Adwani, P.S. Preparation and characterization of copper oxide nanoparticles and determination of enhancement in critical heat flux. *Therm. Sci.* **2017**, *21*, 233–242. [CrossRef]

63. Jeong, D.; Jo, W.; Jeong, J.; Kim, T.; Han, S.; Son, M.-K.; Jung, H. Characterization of Cu$_2$O/CuO heterostructure photocathode by tailoring CuO thickness for photoelectrochemical water splitting. *RSC Adv.* **2022**, *12*, 2632–2640. [CrossRef]

64. Attou, L.; Jaber, B.; Ez-Zahraouy, H. Effect of annealing temperature on structural, optical and photocatalytic properties of CuO nanoparticles. *Mediterr. J. Chem.* **2018**, *7*, 308–316. [CrossRef]

65. Al-Jawhari, H.A. A review of recent advances in transparent p-type Cu$_2$O-based thin film transistors. *Mater. Sci. Semicond. Process.* **2015**, *40*, 241–252. [CrossRef]

66. Balık, M.; Bulut, V.; Erdogan, I.Y. Optical, structural and phase transition properties of Cu$_2$O, CuO and Cu$_2$O/CuO: Their photoelectrochemical sensor applications. *Int. J. Hydrog. Energy* **2019**, *44*, 18744–18755. [CrossRef]

67. Mao, Y.; He, J.; Sun, X.; Li, W.; Lu, X.; Gan, J.; Liu, Z.; Gong, L.; Chen, J.; Liu, P.; et al. Electrochemical synthesis of hierarchical Cu$_2$O stars with enhanced photoelectrochemical properties. *Electrochim. Acta* **2012**, *62*, 1–7. [CrossRef]

68. Patil, P.; Nakate, U.T.; Nakate, Y.T.; Ambare, R.C. Acetaldehyde sensing properties using ultrafine CuO nanoparticles. *Mediterr. J. Chem.* **2019**, *101*, 76–81. [CrossRef]

69. Xu, L.; Li, J.; Sun, H.; Guo, X.; Xu, J.; Zhang, H.; Zhang, X. In situ growth of Cu_2O/CuO nanosheets on Cu coating carbon cloths as a binder-free electrode for asymmetric supercapacitors. *Front. Chem.* **2019**, *7*, 420. [CrossRef] [PubMed]

70. Jansen, R.J.J.; van Bekkum, H. XPS of nitrogen-containing functional groups on activated carbon. *Carbon* **1995**, *33*, 1021–1027. [CrossRef]

71. Wang, P.; Liu, Z.; Han, C.; Ma, X.; Tong, Z.; Tan, B. Cu_2O/CuO heterojunction formed by thermal oxidation and decorated with Pt co-catalyst as an efficient photocathode for photoelectrochemical water splitting. *J. Nanoparticle Res.* **2021**, *23*, 268. [CrossRef]

72. Liu, S.; Hou, H.; Liu, X.; Duan, J.; Yao, Y.; Liao, Q. High-performance hierarchical cypress-like $CuO/Cu_2O/Cu$ anode for lithium ion battery. *Ionics* **2017**, *23*, 1075–1082. [CrossRef]

73. Tariq, M.; Afzal, N.; Rafique, M. Enhanced photodetection performance of sputtered cupric oxide thin film through annealing process. *Opt. Quantum Electron.* **2021**, *53*, 685. [CrossRef]

74. Wang, P.; Ng, Y.H.; Amal, R. Embedment of anodized p-type Cu_2O thin films with CuO nanowires for improvement in photoelectrochemical stability. *Nanoscale* **2013**, *5*, 2952–2958. [CrossRef] [PubMed]

75. Liu, H.; Wang, A.F.; Sun, Q.; Wang, T.; Zeng, H. Cu nanoparticles/fluorine-doped tin oxide (FTO) nanocomposites for photocatalytic H_2 evolution under visible light irradiation. *Catalysts* **2017**, *7*, 385. [CrossRef]

76. Gelderman, K.; Lee, L.; Donne, S.W. Flat-band potential of a semiconductor: Using the Mott–Schottky equation. *J. Chem. Educ.* **2007**, *84*, 685. [CrossRef]

77. Bengas, R.; Lahmar, H.; Redha, K.M.; Mentar, L.; Azizi, A.; Schmerber, G.; Dinia, A. Electrochemical synthesis of n-type ZnS layers on $p-Cu_2O/n-ZnO$ heterojunctions with different deposition temperatures. *RSC Adv.* **2019**, *9*, 29056–29069. [CrossRef]

78. Kim, D.; Zhang, Z.; Yong, K. Synergistic doping effects of a $ZnO: N/BiVO_4$: Mo bunched nanorod array photoanode for enhancing charge transfer and carrier density in photoelectrochemical systems. *Nanoscale* **2018**, *10*, 20256–20265. [CrossRef] [PubMed]

79. Radecka, M.; Rekas, M.; Trenczek-Zajac, A.; Zakrzewska, K. Importance of the band gap energy and flat band potential for application of modified TiO_2 photoanodes in water photolysis. *J. Power Sources* **2008**, *181*, 46–55. [CrossRef]

80. Zhang, Z.; Yu, Y.; Wang, P. Hierarchical top-porous/bottom-tubular TiO_2 nanostructures decorated with Pd nanoparticles for efficient photoelectrocatalytic decomposition of synergistic pollutants. *ACS Appl. Mater. Interfaces* **2012**, *4*, 990–996. [CrossRef]

81. Zhang, Z.; Wang, P. Highly stable copper oxide composite as an effective photocathode for water splitting via a facile electrochemical synthesis strategy. *J. Mater. Chem. A* **2012**, *22*, 2456–2464. [CrossRef]

82. Sivula, K.; Le Formal, F.; Grätzel, M. Solar water splitting: Progress using hematite ($\alpha-Fe_2O_3$) photoelectrodes. *ChemSusChem* **2011**, *4*, 432–449. [CrossRef] [PubMed]

83. Annamalai, A.; Subramanian, A.; Kang, U.; Park, H.; Choi, S.H.; Jang, J.S. Activation of hematite photoanodes for solar water splitting: Effect of FTO deformation. *J. Phys. Chem. C* **2015**, *119*, 3810–3817. [CrossRef]